ADVANCED ELECTRONIC MATERIALS Open Access
www.advelectronicmat.de

Peculiarities of the SCLC Effect in Gate-All-Around Silicon Nanowire Field-Effect Transistor Biosensors

*Yongqiang Zhang, Nazarii Boichuk, Denys Pustovyi, Valeriia Chekubasheva, Hanlin Long, Mykhailo Petrychuk, and Svetlana Vitusevich**

High-quality liquid gate-all-around (LGAA) silicon nanowire (NW) field-effect transistor (FET) biosensors are fabricated and studied their properties in 1 mM phosphate-buffered saline solution with pH = 7.4 using transport and noise spectroscopy. At small V_{DS}, the conventional current behavior of FET with a linear dependence on voltage is registered in the output current-voltage (I-V^M) characteristics with $M = 1$. At drain-source voltage $V_{DS} > 0.6$ V, the I-V characteristics with stronger power M are revealed. It is shown that the current in LGAA NW FETs follows current proportional to voltage in power $M = 4$ dependence on small liquid gate voltages. Transport and noise spectroscopy analyses demonstrate that the obtained results are associated with the space-charge-limited current (SCLC) effect. Moreover, a strong two-level random telegraph signal (RTS) is found in the region corresponding to SCLC at V_{DS} values exceeding 0.6 V. The RTS related to single trap phenomena results in a well-resolved Lorentzian component of noise spectra. The results demonstrate that the SCLC and two-level RTS phenomenon are correlated effects. They should be taken into account during the development of single-trap-based devices, including biosensors.

1. Introduction

The applications of nanoscale biosensors in different fields are increasingly attracting the attention of researchers. The advantages of nanowire (NW) field-effect transistor (FET) sensors are ultrahigh sensitivity and label-free sensing, which allows the detection of various diseases in the fight to prevent them and to preserve human health.[1–5] To obtain reliable detection results, the research community is developing advanced technology for NW FET fabrication and aiming to identify precise parameters for test data analysis. Indeed, beneficial information may come from the dynamic processes of ions at the solid/liquid interface at different applied voltages during the measurements.[6,7] To obtain a high-performance working regime for FET biosensors, the peculiarities of charge carrier behavior in physiological liquids must be studied.[8,9] The space-charge-limited current (SCLC) and random telegraph signal (RTS) caused by a trap near the nano-channel must be studied in detail[1,10–13] for several applications. The characteristic times of RTS are demonstrated as new parameters, which should be considered to obtain enhanced sensitivity in biosensing applications.[1,14,15]

The SCLC regime plays a very important role in the transport of carriers in NW FET structures, as described in numerous reports. This regime was found in the nano-channel structure of GaN, InAs, CdS, ZnO, and GaAs.[10,11,16–18] Usually, the SCLC phenomenon is caused by a change in the concentration of charge carriers in nanowires, the change in the concentration of active charge traps, or the reduced density of thermal equilibrium carriers. The SCLC effect influences the electrical characteristics of FET structures, leading to the superlinear behavior of the I-V curve, described by the Mott-Gurney law, proportional to voltage with an exponent equal to 2[16,19–21] in bulk, film, nanoribbon, and nanowire samples. The SCLC phenomenon does not just influence the static electrical properties of transistors, but also the dynamic noise properties of devices.[22]

To analyze the SCLC effect, the slope of the output I-V curve should be considered in double logarithmic coordinates. Usually, a slope ≈1 is typically indicative of linear ohmic behavior in a low-bias regime. This is followed by a slope ≥2 in the nonlinear SCLC regime. It has been shown[16] that slope ≈2 reflects an absence of active traps in the semiconductor or a single discrete trap level, and that slope >2 is caused by the distribution of partially occupied trap states in a range of energies. Yu et al. found for the GaSb nanowire transistor that the slope of the I-V curve changed after annealing from 3.8 to 1.9. This was due to the SCLC occurring when the number of injected carriers was larger than thermally

Y. Zhang, N. Boichuk, D. Pustovyi, V. Chekubasheva, H. Long, M. Petrychuk, S. Vitusevich
Institute of Biological Information Processing (IBI-3)
Forschungszentrum Jülich
52425 Jülich, Germany
E-mail: s.vitusevich@fz-juelich.de
Y. Zhang, N. Boichuk, D. Pustovyi, S. Vitusevich
Experimentelle Physik 2
Technische Universität Dortmund
44227 Dortmund, Germany

The ORCID identification number(s) for the author(s) of this article can be found under https://doi.org/10.1002/aelm.202300855

DOI: 10.1002/aelm.202300855

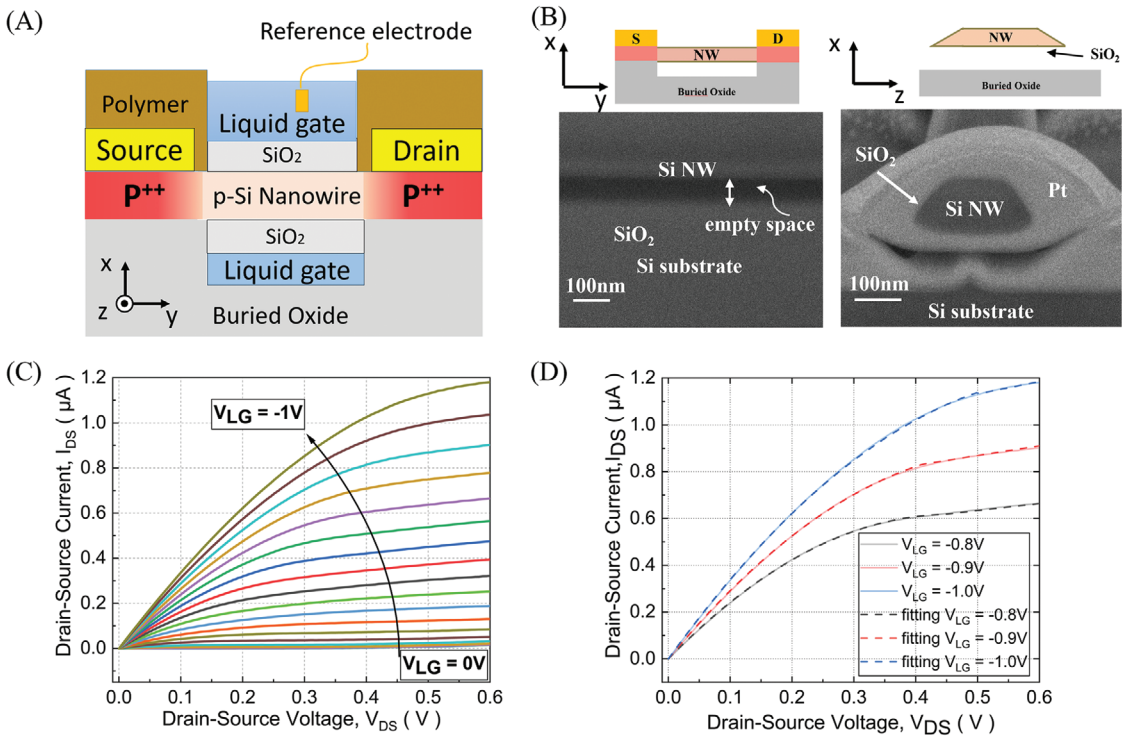

Figure 1. A) Schematic presentation of the cross section of LGAA NW FET. B) FIB cut of fabricated GAA nanowires, demonstrating the nanowire cross-section size. The insets represent schematic GAA FET after fabrication, before introducing volume for a liquid. C) Typical output *I-V* characteristics, registered at ($|V_{DS}| < 0.6$ V) and $V_{LG} > V_{TH}$ obtained for a 2 μm long and 150 nm wide nanowire in 1 mM PBS solution with pH = 7.4 at V_{LG} ranging from 0 to -1 V with a step of 50 mV. D) Calculated *I-V* characteristics according to equation (1) confirm the conventional behavior of measured output characteristics. The fitting parameters are listed in the table below.

generated carriers.[23] They showed that thermally generated carriers dominate the conduction, thus reducing the SCLC effect. Pehrsson et al. first reported the conduction mechanism related to the SCLC in heterostructure nanowires with an output *I-V* characteristic slope of 3.1, plotted in logarithmic scales to analyze the traps of the structure.[24] Moreover, the results demonstrate that the traps are distributed in energy and do not accumulate near a single energy level.

Noise spectroscopy is a powerful method to evaluate the performance of transistors. Guo et al. analyzed noise spectra to demonstrate the obvious transformation behavior from 1/f to $1/f^{1.5}$, which confirms that the SCLC effect occurs in biosensors and reflects the dynamic process of ions at the solid/liquid interface.[22] In nanoscaled NW FETs, when Lorentzian is registered in noise characteristics, this may correspond to the RTS due to single trap phenomena (STP). Kutovyi et al. indicated that parameters of the RTS found as a result of a single trap capturing and emitting the charge carrier near the Si/SiO_2 interface, can be suggested as a new approach. Since the capture time to the trap is ultra-sensitive to changes in surface potential, this allows significant improvement in the biosensor sensitivity compared to the standard current approach utilizing change in the threshold voltage.[1] Therefore, studies of parameters of STP in silicon nanowire-based biosensors show great potential for single-trap-based devices and their application in various research fields, including biomedical applications.

In this work, liquid gate-all-around FETs were fabricated using NW channels with a length of 2 μm and width of 150 nm. The Si NW channels are fabricated using silicon-on-insulator (SOI) wafers with an impurity concentration of 1×10^{15} cm^{-3}. To obtain ohmic contacts source and drain regions were implanted with boron atoms (energy 6 keV, dose 1×10^{15} cm^{-2}), which resulted in p-type transistor structures (p++-p-p++). The contact resistance estimated using the transmission line model[25] was found to be negligibly small (≈4 kΩ), corresponding to about 1.2% of the total resistance of a GAA FET. The NW FETs were studied in 1 mM PBS at pH = 7.4. According to our experimental results, the transistor current consists of the typical FET current component ($I \sim V^M$), where $M = 1$ and the SCLC-induced current components where $M > 1$. The SCLC-induced current registered at $|V_{DS}| >$ 0.6 V was systematically analyzed in LGAA NW FETs using measured *I-V* curves, noise spectroscopy, and RTS fluctuations as a result of STP.

2. Results and Discussions

The schematic presentation of LGAA NW FET devices studied here is shown in **Figure 1**A. Current-voltage characteristics and noise spectra of LGAA NW FET were measured at different drain-source voltages (V_{DS}) and different liquid-gate voltages (V_{LG}) in 1 mM PBS solution. Using a focused ion beam (FIB) cut (Figure 1B), the free-standing state of the nanowire is confirmed, and the diameter of the NW channel was found to be ≈150 nm.

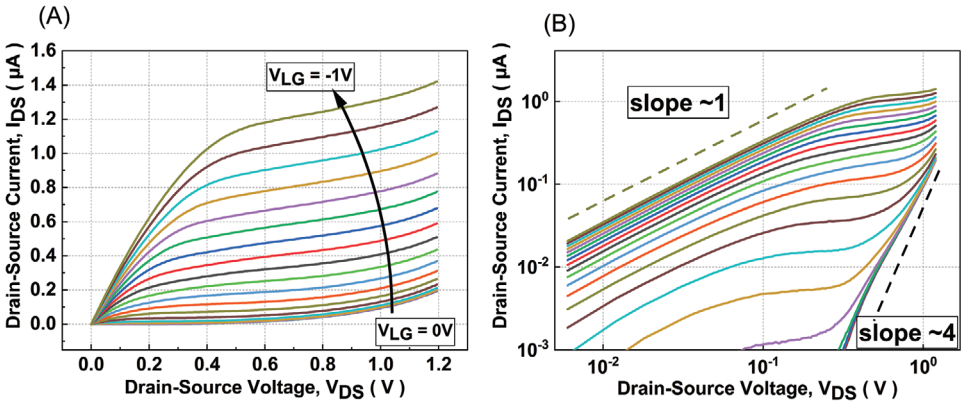

Figure 2. A) Typical output *I-V* characteristics registered for V_{DS} whole range, including $|V_{DS}| > 0.6$ V and $V_{LG} > V_{TH}$ obtained for 2 μm long and 150 nm wide nanowire in 1 mM PBS solution with pH = 7.4 at V_{LG} ranging from 0 to -1 V with a step of 50 mV. B) The output *I-V* curves of Figure 2A show in the log-log scale two different slopes of 1 and 4.

It should be noted that for FIB cut studies, the nanowires were covered with a thin platinum, Pt, layer.

2.1. Current-Voltage Characteristics of LGAA NW FET

Typical output characteristics measured for LGAA NW FET at small voltages ($|V_{DS}| < 0.6$ V) are shown in Figure 1C. For low voltages, a conventional *I-V* characteristic for NW FET was obtained, containing the linear characteristic $I \sim V^M$, where M is equal to 1 followed by the saturation region. The conventional drain-source current I_{DS} as a function of V_{LG} and V_{DS} of FET device was fitted in different operation regions using the following equation:

$$I_{DS} = \begin{cases} 0, \ V_{LG} \le V_{TH}; \\ C_{ox}\mu\frac{W}{L}\left[\left(V_{LG}-V_{TH}\right)V_{DS}-\frac{1}{2}V_{DS}^2\right], \quad V_{LG} > V_{TH}, V_{DS} \le V_{LG}-V_{TH}; \\ \frac{1}{2}C_{ox}\mu\frac{W}{L}\left(V_{LG}-V_{TH}\right)^2\left[1+\lambda\left(V_{DS}-V_{DSsat}\right)\right], \ V_{LG} > V_{TH}, V_{DS} > V_{LG}-V_{TH}. \end{cases} \tag{1}$$

where V_{TH} is the threshold voltage, μ is the electron mobility, C_{ox} is the capacitance of the oxide layer covering NW and separating the nanowire from direct contact with a liquid, λ is the nano-channel length modulation parameter, V_{DSsat} is the saturation V_{DS}, and W and L are the width and length of the nano-channel, respectively.

Table 1. List of fitting parameters used for the analysis of conventional *I-V* output characteristics of LGAA NW FET with a 2 μm long and 150 nm wide nanowire. $C_{OX} = 0.0017$ F m^{-2}; μ = 50 cm^2 V^{-1}s^{-1}, extracted directly from measured transfer characteristics similar as described.[26]

V_{LG} [V]	V_{OD} [V]	V_{TH} [V]	λ	V_{DSsat} [V]
0.80	0.45	0.35	0.48	0.43
0.90	0.55	0.35	0.48	0.55
1.00	0.65	0.35	0.48	0.65

Here V_{OD} is the overdrive voltage, estimated as $V_{OD} = V_{LG} - V_{TH}$.

The results of I_{DS} behavior are in good agreement with *I-V* as described by equation (1). It should be noted that the output I-V curves are symmetric with respect to a point $V_{DS} = 0$ V, $I_{DS} = 0$ in the range from −0.1 to 0.1 V, demonstrating high-quality fabricated ohmic contacts. Typical fitted *I-V* characteristics obtained for several liquid-gate voltages are shown in Figure 1D. The fitting parameters are listed in **Table 1**.

Interesting features were registered in the output *I-V* characteristics at relatively high drain-source voltages ($|V_{DS}| > 0.6$ V), as shown in **Figure 2A**. A specific growth trend was registered after the saturation region. The *I-V* curves change their shape and slope with increasing liquid-gate voltage (V_{LG}), as shown by the data in Figure 2B where the output *I-V* characteristics are plotted in a log-log scale. It can be introduced as the critical characteristic voltage (V_C), i.e., the voltage, at which the *I-V* curves change from linear to superlinear behavior. When the V_{LG} is below the V_C, the *I-V* curve only shows a conventional trend and can be described using standard equations for FET devices. At the same time, when the V_{LG} is above V_C, the *I-V* curve can be analyzed in two parts: the conventional FET curve and the second rising part, which are easy to distinguish. The rising component of current, obtained at $V_{LG} = 0$ V is introduced here as I_0. Subsequently, subtracting I_0 from the remaining curves results in the conventional output curves.

To analyze the rising part of the output curves, the double logarithmic scale of *I-V* curves was very useful. When the liquid-gate voltage was zero, a considerable increase in drain current was registered at a voltage of −0.4 V. The slope was ≈4. Usually, *I-V* characteristics with a slope of 2 in the bulk material are related to the space charge limited current (SCLC) effect. The SCLC effect can be explained by the injection of carriers from the contact regions not only in bulk materials but also in nanostructures, including nanowires. SCLC can be described by the Mott-Gurney law[27] as follows:

$$I_D = \zeta\frac{\varepsilon\mu V_{DS}^2}{4\pi L} \tag{2}$$

where ζ is the coefficient of the order of unity, ϵ is the permittivity, μ is the mobility of free current carriers, and L is the length of the nanowire.

However, a considerably strong slope was registered in the trap-filling limit voltage regime:[18]

$$I \sim V_{DS}^{M} \tag{3}$$

with M considerably exceeding power 2.

A. Rose discussed the SCLC effect using the nonlinear shape of the I-V curve, which is caused by traps in insulators.[28] He demonstrated that the I-V curve deviates from an ideal quadratic law and shows a much higher power dependence on drain-source voltage. The phenomenon of a higher power (>2) dependence on voltage can be explained by the peculiarities in the energy distribution of traps.[1] Saied et al. employed the device structure of $Al_{0.3}Ga_{0.7}As/In_{0.15}Ga_{0.85}As/GaAs$ to study SCLC. They found excess conduction under $V_{DS} > 2.5$ V and a soft pinch-off at a high V_{DS} range measured at a temperature of 300 K.[29] It should be noted that the SCLC phenomenon can be controlled by traps[1] in the channel of the structures, ensuring the excess output conductance and a specific upward trend of the I-V curve. Usually, with an increase in V_{DS}, the traps in the nano-channel can be filled, leading to an upward shift of the quasi-Fermi level. An obvious rise in I_{DS} when the V_{DS} reached the trap-filling limit voltage regime[18] was demonstrated.

Our results (Figure 2B) demonstrate well-resolved superlinear dependence on the applied voltage V_{DS} with a slope of ≈4. This slope is related to the SCLC effect, as confirmed by our other results discussed below. It should be noted that a slope exceeding 1 in I-V curves can be effectively used to obtain enhanced sensitivity of LGAA NW FET biosensors[22] in the presence of the SCLC effect in the nano-channel. At the same time, the slope of the superlinear part in I-V characteristics decreases gradually from the initial value of ≈4 as V_{LG} increases due to a stronger contribution of the main current in the nanowire channel. When V_{LG} changes, charge states on the surface of the LGAA channel also control the intensity of the interaction of nano-channel carriers with traps. Traps in the SiO_2 layer near the Si/SiO_2 interface with a small channel diameter may assist in forming a strong dependence $I \sim V^M$ with $M > 2$ in our NW FETs working with a liquid gate, i.e in the case then the nano-channel is surrounded by a liquid.

Noise spectroscopy is a powerful method for analyzing trap centers in materials and devices.[30] Therefore, we used noise spectroscopy to study the increased section of the I-V characteristics related to the SCLC effect for sensors working in the liquid environment.

2.2. Noise Spectra of LGAA NW FET Structures

To investigate the relation between SCLC-induced current and dynamics due to traps in SiO_2 (gate oxide contacting with PBS solution) near the Si/SiO_2 interface in LGAA NW FETs, we measured the noise spectra in 1 mM PBS solution at pH = 7.4 at different voltages. **Figure 3A** illustrates the typical power spectral density (S_V) of the drain voltage for a FET device with a nanowire length and width of 2 μm and 150 nm, respectively. The measurements were performed at constant $V_{LG} = -0.2$ V and different ranges of V_{DS} from −0.1 to −1.2 V. It should be noted that part of the measured noise spectra corresponds to conventional I-V characteristic behavior. However, noise spectra obtained for the voltage range above 0.6 V demonstrate additional Lorentzian peaks. This deviation in noise spectra correlates well with deviation in I-V characteristics from the linear dependence to current proportional $I = V^M$, with $M > 1$ corresponding to the region reflecting the SCLC effect.

The Lorentzian peaks can be described by the following equation:

$$S_V(f) = \frac{S_V(0)}{1 + (2\pi f \tau)^2} \tag{4}$$

where $S_V(f)$ is the voltage noise spectral density at frequency f, $S_V(0)$ − the same value at $f \to 0$, τ − time constant of generation-recombination (GR) fluctuations.

By plotting S_V as a function of frequency, f, (Figure 3B) the Lorentzian component[1] can be analyzed by finding their characteristic time constant in noise spectra, $S_V(f)$. In our samples, such Lorentzian peaks are very well resolved at V_{DS} values exceeding −0.6 V in the noise spectra. The time constant of GR fluctuations was estimated using Equation (4) to be in the order of 40 μs. It should be noted that in the case of NW FET containing not only a liquid gate but also a metal back gate the channel position can be moved far away from the dielectric layer contacting with a liquid. This considerably reduces noise level due to changes in mechanisms determining noise origin.[25]

In nanosized device structures, the Lorentzian is closely related to random telegraph signal (RTS) noise due to the capture and emission of charge carriers by the single trap located in the dielectric layer near the Si/SiO_2 interface. The RTS phenomenon appears at the same voltages as the SCLC effect registered in the I-V characteristics, i.e., at high V_{DS} values.

The time constant of the Lorentzian is related to capture and emission time constants as follows:

$$\tau = \frac{\tau_c \cdot \tau_e}{\tau_c + \tau_e} \tag{5}$$

where τ_c is the capture time, τ_e is the emission constant in the channel of the LG NW FET structure.

It is well known that two-level RTS noise represents an important method to study charge carrier dynamics in dielectric layers contacting a liquid and single trap phenomena (STP).[12] The fluctuations of I_{DS} recorded at high values of V_{DS} using an in-house noise measurement system are shown in Figure 3C. The amplitude of I_{DS} increases in a range of V_{DS} from −0.6 to −1.2 V. It should be noted that the starting voltage was $V_{DS} = -0.8$ V when RTS was found in PBS solution with pH = 7.4. This demonstrates the relation between two-level RTS and the SCLC when most of the traps are filled by carriers captured from the NW channel. Thus, the SCLC effect plays a role in the relatively large amplitude of RTS at a higher negative V_{DS} (i.e., $V_{DS} < -0.6$ V).

The statistical histogram is a very effective method of analyzing two-level RTS noise. Figure 3D displays I_{DS} histograms obtained using time traces. Two Gaussian peaks gradually become more distinguishable as V_{DS} increases. They very well separate into two peaks at high voltages. The peaks represent the emission and capture states of the single trap.

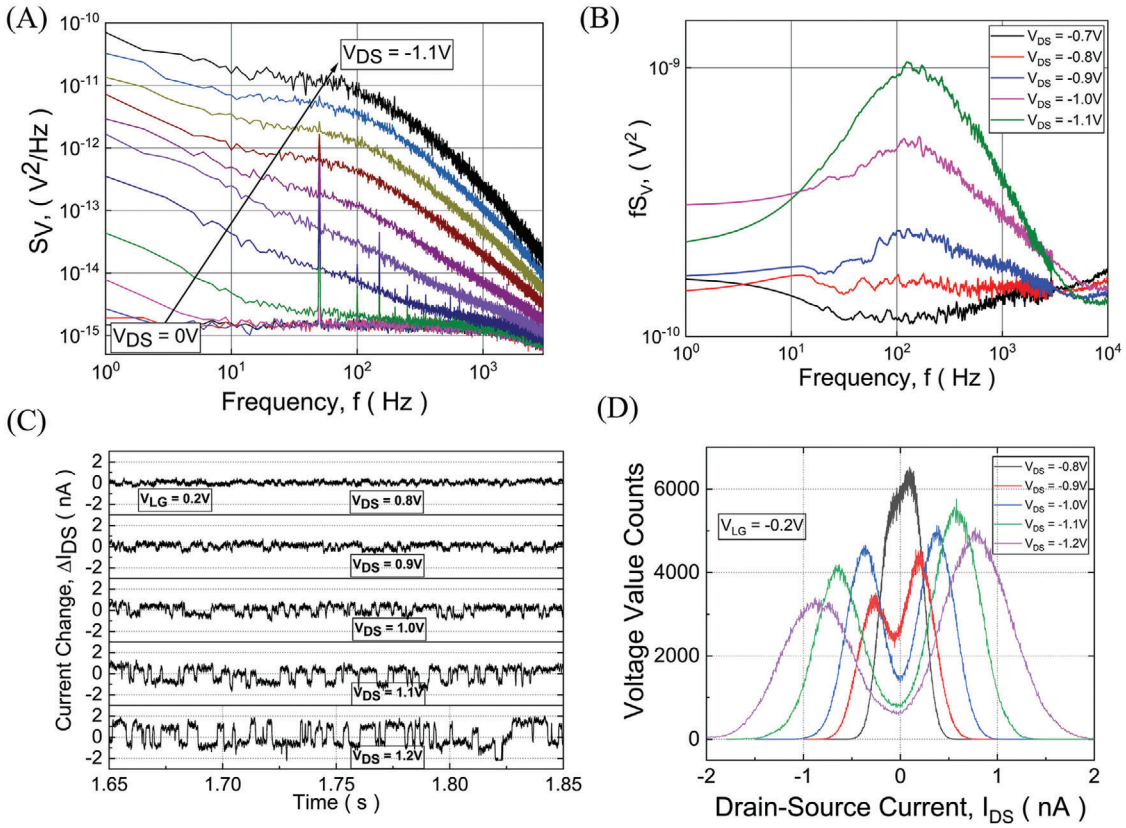

Figure 3. A) The voltage spectral density measured for a nanowire with a length of 2 µm and width of 150 nm at different V_{DS} with a step of 0.1 V and at a constant V_{LG} of −0.2 in PBS solution. B) Normalized noise spectra density measured at different V_{DS} and at $V_{LG} = -0.6$ V, Lorentzian noise components registered at relatively large voltages V_{DS}. C) The two-level RTS measured for a nanowire with a length of 2 µm and width of 150 nm in drain current I_{DS} are recorded at different V_{DS} at constant $V_{LG} = -0.2$ V. D) Histograms, obtained using RTS time traces, demonstrating the current amplitude as very well separated in Gaussians peaks due to STP.

It should be noted that the ratio between the capture time constant and emission time constant τ_e/τ_c represents the dimensionless parameter R. **Figure** 4A shows the R-factor dependence on V_{DS}, which can be recalculated as a function of I_{DS} (Figure 4A,B). The R-factor changes by 30% as the V_{DS} applied to the LGAA NW FET structure increases. With an increase in V_{DS} or I_{DS}, the R-factor tends to decrease. This indicates a possible accumulation of a larger concentration of charge carriers in the transistor nano-channel. The accumulation of charge in the nanowire channel can lead to an increase in the nonuniformity

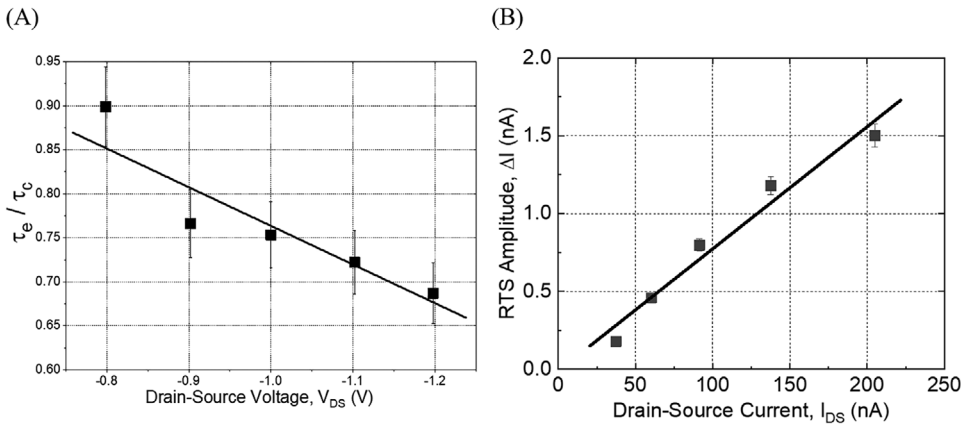

Figure 4. A) The ratio of τ_e/τ_c plotted against V_{DS} at a V_{LG} value of −0.2 V, obtained for a nanowire with a length of 2 µm and width of 150 nm. B) The amplitude of RTS current as a function of I_{DS} corresponds to the V_{DS} range from −0.8 to −1.2 V at $V_{LG} = 0$, obtained for a nanowire with a length of 2 µm and width of 150 nm in 1 mM PBS solution at pH = 7.4.

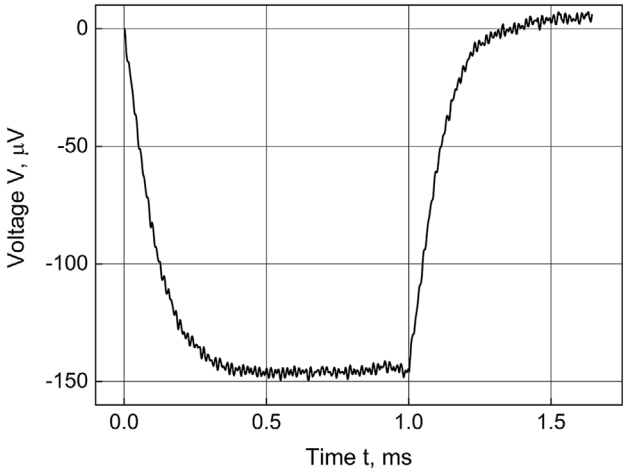

Figure 5. Typical time trace obtained by averaging 100 fluctuations of the RTS signal measured for a nanowire with a length of 2 μm and width of 150 nm at $V_{LG} = -0.2$ V and at $V_{DS} = -1.1$ V.

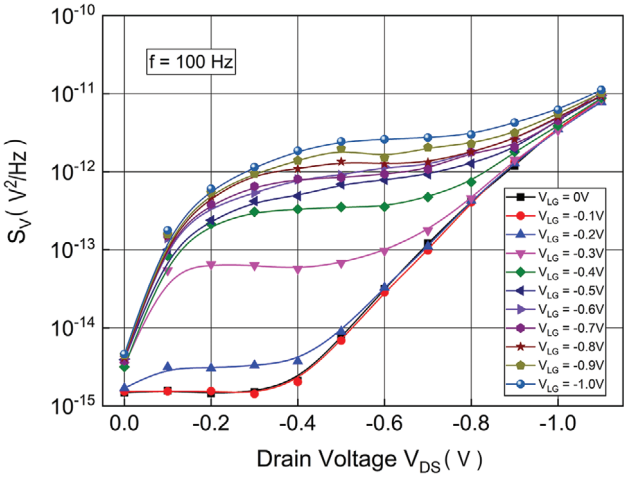

Figure 6. Voltage spectral density, S_V flicker noise component, as a function of voltage, obtained at 100 Hz from noise spectra measured for a nanowire with a length of 2 μm and width of 150 nm in PBS solution with pH = 7.4 at different V_{LG} values.

of the redistribution of carriers along the NW channel as a result of the SCLC effect. With an increase in V_{DS}, significant charge redistribution in the nano-channel causes an increase in the amplitude of the two-level RTS. This result confirms that the RTS phenomenon and the SCLC observed for $V_{DS} = -0.6$ V are correlated effects.

Figure 4 shows the amplitude of RTS (ΔI_{DS}) due to the STP, obtained from recorded time traces, as a function of I_{DS} currents, measured in the V_{DS} range from −0.8 to −1.2 V at various V_{LG} voltages. As the I_{DS} current increases, all curves tend to increase. This can be explained by the following considerations. The local charge density temporarily changes as a result of the modulation of channel conductivity by an electron captured by the trap near the nanowire Si/SiO_2.[12–14,31,32] These variations in the electric field in the nanowire channel lead to stronger I_{DS} fluctuations at large V_{DS} values.

It should be noted that the SCLC-induced current appears at relatively high V_{DS}. At these voltages, the two-level RTS phenomenon is observed in biosensors. It can be concluded that the SCLC effect assists in registering the RTS at high V_{DS} voltages.

The shape details of the STP-related component were analyzed using the statistical behavior of the RTS signals shown in **Figure 5**.

The data allow us to estimate the capacitance related to the SCLC effect as follows. The relaxation time constant, τ, can be estimated using fronts of the time trace pulses reflection two-level current fluctuations (Figure 5) at the level $1/e$ from the starting voltage of the pulse. It is estimated to be 113 μs. Then, the capacitance of the LGAA NW FET device due to carrier redistribution in the channel as a result of the SCLC effect can be estimated using the relaxation time constant as follows:

$$\tau = RC \tag{6}$$

where R is the resistance of the sample, estimated using *I-V* characteristic at $V_{LG} = -0.2$ V and at $V_{DS} = -1.1$ V.

The capacitance of the LGAA NW FET was found to be 22 pF. Here C is the capacitance due to a single trap situated in SiO_2 layer near Si/SiO_2 interface.

In addition, the noise characteristic is a useful tool to investigate the charge carrier behavior on the surface of a nanowire in a liquid environment. Therefore, the normalized voltage spectral density S_V values corresponding to the flicker component of noise at 100 Hz, determined for different liquid-gate voltages, were obtained using noise spectra measured in PBS solution. **Figure 6** shows S_V as a function of V_{DS} voltage, obtained at a frequency of 100 Hz plotted on a semi-logarithmic scale. It should be noted that the minimum level of noise ($\approx 1.5 \cdot 10^{-15}$ V^2s) corresponds to the thermal noise level described as follows:

$$S_{\text{Thermal}}(f) = 4KTR_{eq} \tag{7}$$

where R_{eq} is the input resistance of the low-noise amplifier, K is the Boltzmann constant, and T is the temperature.

As can be seen in Figure 6, the data demonstrate a strong dependence of S_V on V_{DS}, in the range of small V_{DS} values ($|V_{DS}| <$ 0.6 V). At the same time, for voltages above 0.6 V, almost no changes (within one order of magnitude) were registered. The data in Figure 5 show a strong redistribution of carriers along the channel due to injected carriers and the formation of a sharp step in carrier redistribution. The step defines the capacitance formation, the value of which is determined using the exponential behavior of fronts of the pulse (Figure 5) as 22 pF.

In addition, when current flows through the device nanochannel, the charge carrier dynamic process explains the S_V behavior.[33] These changes can provide valuable information on the sources of dynamic fluctuations extracted from noise spectra. In our LGAA NW FET samples, two Lorentzian noise components were registered in the measured noise spectra. The two-level RTS fluctuations were found to correspond to Lorentzian noise components. The RTS was excited in a high electric field region, where the SCLC is registered. The fact indicates that almost all traps are filled except a single trap determining the RTS

noise signal. The SCLC effect was registered with a slope $M \sim 4$ in the output *I-V* curves in a double logarithmic scale at a high V_{DS} range from −0.6 V to −1.2 V. Thus, the SCLC effect, which is important for biosensing applications, can be studied using a new approach represented by the RTS fluctuations and corresponding Lorentzian components in noise spectra to find more suitable parameters for biosensing detections. The results imply that further investigation of the SCLC effect is important for the development of advanced device structures and biosensor technologies.

3. Conclusion

In summary, we investigated the electrical and noise characteristics of fabricated LGAA NW FET biosensors in PBS solution. We found that at small voltages, the current of the LGAA transistor reflects conventional FET behavior. At drain-source voltages ($|V_{DS}|$) above 0.6 V, deviation from conventional behavior was found. We determined the slope of the *I-V* characteristics as 4 in double logarithmic scale in the high V_{DS} voltage range and for small V_{LG} values. Our results on the transport and noise property measurements of LGAA NW FET biosensors indicate the formation of a transport regime corresponding to the SCLC effect. Moreover, the noise measurement revealed the two-level RTS phenomenon in the same voltage range, where the SCLC effect is resolved in *I-V* characteristics. We propose a new approach for SCLC analysis using RTS characteristic times. Analyzing the shape of RTS fluctuations allowed the determination of the characteristic capacitance as a result of the SCLC effect as 22 pF. The RTS related to STP and noise spectroscopy provide valuable information on the SCLC effect in LGAA NW FET. The results should be taken into account for the development of single-trap-based nanotransistor structures, including biosensors.

4. Experimental Section

The silicon-on-insulator (SOI) wafer ($N_A = 10^{15}$ cm^{-3}) was cleaned by a full RCA clean. Next, the hard mask of 20 nm SiO_2 was formed on the clean Si surface via thermal oxidation at 900 °C. After this, nanowires and alignment markers were patterned using electron-beam lithography (EBL) after spin coating of positive photoresists UV-6 on the dielectric layer at 4000 rpm for 45 s, followed by baking at 130 °C for 1 min. Then, the tetramethylammonium hydroxide (TMAH) solution was applied at 80 °C to a surface. Wet etching was chosen instead of dry etching as it provides a low surface roughness of the nanowire. To obtain good ohmic contact in the drain, source, and back gate regions of the devices were implanted with boron ions (p-type), using an energy of 6 keV and dose of 10^{15} cm^{-2} at a tilt angle of 7°. Rapid thermal annealing (RTP) was used to anneal the transistors at 1000 °C for a short time to get an outstanding ohmic contact. An additional 8 nm SiO_2 was deposited to protect the nanowires during thermal oxidation. The GAA structures were obtained from the SOI substrate by immersing them in buffered oxide etch (BOE 7:1) for 25 s. The metal feed lines connected the drain and the source contacts to contact pads at the edges of the chip for electrical and noise characterization. For metallization of the contacts and feed lines, thermal evaporation was employed to deposit 5 nm Ti and 200 nm Al on the entire sample surface, followed by the lift-off process and RTP at 450 °C for 10 min. For the passivation step, the adhesion promoter, polyimide, and photoresist were applied to the surface of the devices by spin coating. The opening windows above the nano-channel were made using photolithography. They provide access for the test liquid to the nanowire surface during measurements. Subsequently, samples were diced to the desired size and then glued with silver paste to the chip carrier. Then, contact pads on the chip were wired to contacts on the chip carrier via the bonding system. Finally, two concentric glass rings were attached to the chip surface with polydimethylsiloxane (PDMS) to form the open container for the test liquid around the location of the transistors. PDMS, serving also as an encapsulation material, covered the area on the sample between the glass rings to protect the contacts and bonds from the liquid.

Characterizations: To avoid the influence of external electromagnetic radiation on the noise and electrical characteristics, we used a metal Faraday cage to cover the sample holder. The Keithley 2400 source measurement unit was employed to investigate the signal of voltage and current during the detection. Here, the reference electrode is Ag/AgCl, which should be submerged in the solution during the measurements and used as a liquid gate. It should be noted that we used an in-house noise measurement system to test the transistors. A potentiometer and rechargeable battery supplied biases to V_{DS} and V_{LG}, respectively. The valuable noise spectra were measured in the range of 1 Hz to 100 kHz using the in-house measuring system, containing a series of amplifiers, and analyzed as noise spectra density using Fourier transformation.

Statistical Analysis: For statistical analysis, the useful noise signal separation should be mentioned due to the various noises that can be recorded during the measurements. It is critical to avoid the effect of thermal noise on the results before any processing of initial noise data $S_v(f)$. The thermal noise $S_{Thermal}(f)$ as a function of equivalent resistance R_{eq} is given by:

$$S_{V\_Thermal}\ (f) = 4KTR_{eq} \tag{8}$$

where the *K* and *T* are the Boltzmann constant and non-zero temperature, respectively. Therefore, by removing the charge carrier thermal excitation noise, the remaining noise is shown in Equation (9).

$$S_{v,real}\ (f) = S_v\ (f) - 4KTR_{eq} \tag{9}$$

To observe the amplitude of current spectral density under different V_{LG} conditions at a frequency of 10 Hz, Equation (10) was employed.

$$S_I\ (f) = \frac{S_{v,real}\ (f)}{R_{eq}^2}\left[\frac{1}{1+\left(\frac{f}{f_P}\right)^2}\right]^{-1} \tag{10}$$

The corner frequency, f_P comes from the parasitic capacitance of the preamplifier input. The observation of the time constants τ_c and τ_e is essential in analyzing the fluctuation of the RTS signal, and the formula is written as:

$$\begin{cases} \tau = \frac{1}{2\pi f_0} \\ \frac{\tau_c}{\tau_e} = \frac{Counts(capture)}{Counts(emission)} \\ \tau = \frac{\tau_c\tau_e}{\tau_c+\tau_e} \end{cases} \tag{11}$$

where f_0 is the noise corner frequency with two-level RTS from the frequency data recorded via the noise system, and the ratio between τ_c and τ_e can be calculated from time traces and using the two Gaussian peaks of the current histogram (e. g. Figure 3 (C)).

The shape of the average RTS pulse is obtained by averaging 50 separate RTS pulses with the same amplitude. The same number of individual pulses was used to obtain the relaxation time τ.

The Lorentzian shape of the two-level RTS spectra can be described using the following equation:

$$S_I\ (f) = \frac{4\Delta I^2}{(\tau_c+\tau_e)\left[\left(\frac{1}{\tau_c}+\frac{1}{\tau_e}\right)^2 + (2\pi f)^2\right]} \tag{12}$$

where the ΔI represents the change in drain-source current due to the single trap near the Si/SiO_2 interface capture and emission process.

Acknowledgements

Y.Z. and H.L. are very grateful for research grants received from the China Scholarship Council (CSC). The authors also thank all the technical staff of the Helmholtz Nano Facility (HNF) of Forschungszentrum Jülich for their assistance with the fabrication of the sensor devices. M.Petrychuk is very grateful for a research grant from the Helmholtz Initiative and networking funds.

Conflict of Interest

The authors declare no conflict of interest.

Data Availability Statement

The data that support the findings of this study are available from the corresponding author upon reasonable request.

Keywords

GAA nanowire, noise spectroscopy, SCLC, single trap phenomena, two-level RTS

Received: December 6, 2023
Revised: March 7, 2024
Published online: April 1, 2024

[1] Y. Kutovyi, H. Hlukhova, N. Boichuk, M. Menger, A. Offenhaeusser, S. Vitusevich, *Biosens. Bioelectron.* **2020**, *154*, 112053.
[2] Y. Cui, Q. Wei, H. Park, C. M. Lieber, *Science* **2001**, *293*, 1289.
[3] M. Wipf, R. L. Stoop, A. Tarasov, K. Bedner, W. Fu, I. A. Wright, C. J. Martin, E. C. Constable, M. Calame, C. Schonenberger, *ACS Nano Lett.* **2013**, *7*, 5978.
[4] T. Sakata, R. Shiratori, M. Kato, *Anal. Chem.* **2022**, *94*, 2820.
[5] N. Clément, K. Nishiguchi, J. F. Dufreche, D. Guerin, A. Fujiwara, D. Vuillaume, *Appl. Phys. Lett.* **2011**, *98*, 264107.
[6] P. Bergveld, *IEEE Trans. Biomed. Eng.* **1972**, *19*, 342.
[7] E. Wernersson, R. Kjellander, J. Lyklema, *J. Phys. Chem. C* **2010**, *114*, 1849.
[8] D. E. Yates, S. Levine, T. W. Healy, *J. Chem. Soc.* **1973**, *70*, 1807.
[9] R. Sivakumarasamy, *Nat. Mater.* **2018**, *17*, 464.
[10] Y. Gu, L. J. Lauhon, *Appl. Phys. Lett.* **2006**, *89*, 14.
[11] A. D. Schricker, F. M. Davidson, R. J. Wiacek, B. A. Korgel, *Nanotechnology* **2006**, *17*, 2681.
[12] Y. Kutovyi, I. Zadorozhnyi, V. Handziuk, H. Hlukhova, N. Boichuk, M. Petrychuk, S. Vitusevich, *Nano Lett.* **2018**, *18*, 7305.
[13] M. Petrychuk, I. Zadorozhnyi, Y. Kutovyi, S. Karg, H. Riel, S. Vitusevich, *Nanotechnology* **2019**, *30*, 305001.
[14] J. Li, S. Vitusevich, M. Petrychuk, S. Pud, A. Offenhäusser, B. Danilchenko, *J. Appl. Phys.* **2013**, *114*, 203704.
[15] J. Li, Y. Kutovyi, I. Zadorozhnyi, N. Boichuk, S. Vitusevich, *Adv. Mater. Interfaces* **2020**, *7*, 15.
[16] A. A. Talin, F. Léonard, B. S. Swartzentruber, X. Wang, S. D. Hersee, *Phys. Rev. Lett.* **2008**, *101*, 076802.
[17] A. A. Talin, F. Léonard, A. M. Katzenmeyer, B. S. Swartzentruber, S. T. Picraux, M. E. Toimil-Molares, J. G. Cederberg, X. Wang, S. D. Hersee, A. Rishinaramangalum, *Semicond. Sci. Technol.* **2010**, *25*, 024015.
[18] P. Zhang, Y. S. Ang, A. L. GAarner, A. Valfells, J. W. Luginsland, *J. Appl. Phys.* **2021**, *129*, 10.
[19] N. F. Mott, R. W. Gurney, *Electronic processes in ionic crystals*, 2nd ed., Clarendon Press, Oxford **1948**.
[20] M. A. Lampert, P. Mark, *Current INjection in Solids*, Academic Press, New York **1970**.
[21] A. A. Grinberg, S. Luryi, M. R. Pinto, N. L. Schryer, *IEEE Trans. Electron Devidces* **1989**, *36*, 1162.
[22] Y. Guo, D. Pustovyi, Y. Kutovyi, N. Boichuk, Y. Zhang, S. Vitusevich, *Adv. Mater. Interfaces* **2022**, *9*, 32.
[23] W. Xu, A. Chin, L. Ye, C. Z. Ning, H. Yu, *J. Appl. Phys.* **2012**, *111*, 10.
[24] B. S. Simpkins, M. A. Mastro, C. R. Eddy, J. K. Hite, P. E. Pehrsson, *J. Appl. Phys.* **2011**, *110*, 4.
[25] S. Pud, J. Li, V. Sibiliev, M. Petrychuk, A. O. V. Kovalenko, S. Vitusevich, *Nano Lett.* **2014**, *14*, 578.
[26] V. Handziuk, Y. Kutovyi, H. Hlukhova, I. Zadorozhnyi, N. Boichuk, M. Petrychuk, S. Vitusevich, ICNF 2019, Neuchatel, Switzerland, 18-21 June **2019**, 269199.
[27] V. A. Sydoruk, I. Zadorozhnyi, H. Hardtdegen, H. Lüth, M. V. Petrychuk, A. V. Naumov, V. V. Korotyeyev, V. A. Kochelap, A. E. Belyaev, S. A. Vitusevich, *Nanotechnology* **2017**, *28*, 135204,
[28] A. Rose, *Phys. Rev.* **1955**, *97*, 1538.
[29] S. Tehrani, H. Goronkin, M. M. Hoogstra, J. A. Curless, G. D. Kramer, M. S. Peffley, P. K. Tsui, *IEEE Trans. Electron Devidces* **1989**, *36*, 1591.
[30] N. B. Lukyanchikova, *Noise Research in Semiconductor Physics*, CRC Press, London **1997**.
[31] Y. Kutovyi, I. Madrid-Canales, N. Boichuk, S. H. Kim, T. Fujii, L. Jalabert, S. V. A. Offenhaeusser, N. Clement, *Jpn. J. Appl. Phys.* **2021**, *60*, 1.
[32] S. Tehrani, H. Goronkin, M. M. Hoogstra, J. A. Curless, G. D. Kramer, M. S. Peffley, P. K. Tsui, *IEEE Trans. Electron Devices* **1989**, *36*, 1591.
[33] Y. Kutovyi, I. Zadorozhnyi, H. Hlukhova, V. Handziuk, A. I. M. Petrychuk, S. Vitusevich, *Nanotechnology* **2018**, *29*, 175202.